

Article

Weak Underwater Acoustic Target Detection and Enhancement with BM-SEED Algorithm

Fan Yin ^{1,2}, Chao Li ^{1,2,*}, Haibin Wang ^{1,2}, Leixin Nie ^{1,2} , Yonglin Zhang ^{1,2}, Chaonan Liu ¹ and Fan Yang ³ 

¹ State Key Laboratory of Acoustics, Institute of Acoustics, Beijing 100190, China

² School of Electronic, Electrical and Communication Engineering, University of Chinese Academy of Sciences, Beijing 100049, China

³ Laboratory of ImViA, University of Burgundy, 21078 Dijon, France

* Correspondence: chao.li@mail.ioa.ac.cn

Abstract: Bearing time record (BTR) is widely used in the field of passive sonar information processing for target detecting and tracking. One of its challenges is to obtain high-resolution beamforming power spectral to facilitate the directions estimating of arrivals, namely DOA estimating. This paper proposes a new algorithm framework Block Matching - Subband Extrema Energy Detection (BM-SEED) to supplement the resolution and enhance the weak targets of BTRs. It extracts the peak features of target trajectories within the conventional beamforming (CBF)-based BTRs by using an improved sub-band peak energy detection (SPED) algorithm, and then enhances the weak targets and suppresses the false-alarm targets through time-spatial autocorrelation analysis. Simulations and sea-trial data evaluations demonstrate that the method of this paper can enhance weak targets, eliminate the interferences of false targets and improve the resolution of BTR targets to 1 degree under -20 dB.

Keywords: weak target enhancement; false target suppression; high resolution; broadband signal processing; passive sonar detection



Citation: Yin, F.; Li, C.; Wang, H.; Nie, L.; Zhang, Y.; Liu, C.; Yang, F. Weak Underwater Acoustic Target Detection and Enhancement with BM-SEED Algorithm. *J. Mar. Sci. Eng.* **2023**, *11*, 357. <https://doi.org/10.3390/jmse11020357>

Academic Editors: Philippe Blondel and Rafael Morales

Received: 23 November 2022

Revised: 22 December 2022

Accepted: 28 January 2023

Published: 5 February 2023



Copyright: © 2023 by the authors. Licensee MDPI, Basel, Switzerland. This article is an open access article distributed under the terms and conditions of the Creative Commons Attribution (CC BY) license (<https://creativecommons.org/licenses/by/4.0/>).

1. Introduction

DOA is one of the most challenging research focuses of array signal processing, which has received extensive attention in recent years. The detection gain of the sonar array is theoretically inversely proportional to the aperture size (Rayleigh limit), thus the resolution of the target detected by the traditional beamforming technology is usually not high enough, so as the weak targets are easily submerged in the background noise. Bartlett [1,2] proposed the conventional beamforming (CBF) method fuses the channel signals into a single beam by compensating them in phase, so that the signal-to-noise ratio (SNR) can be well improved. Capon [3] proposed the MVDR beamformer to obtain a higher array gain and resolution, its goal is to have the beamformer's signal of interest at the output without distortion and with minimal output noise variation. Schmidt [4] and Roy [5] proposed the subspace-based super-resolution algorithms MUSIC and ESPRIT, respectively. However, these two algorithms are limited in practical applications due to their excessive computational effort and parameter requirements.

Bearing time recording (BTR) is a commonly used passive sonar information processing method to spatial spectrum estimation for acoustic target detecting and tracking, which is the accumulation of DOA spectra along the time axis. BTR post-processing methods are therefore developed to further enhance the quality of BTRs in order to facilitate the acoustic detecting and tracking tasks. Bono et al. [6] proposed the subband energy detection (SED) algorithm by combining the SPED and Subband Extrema Energy Detection (SEED). The methods of SED families eliminate the sub-band energy other than local peaks and reduces the influence of noise, thereby improving the bearing resolution and signal detection ability. Ma et al. [7] introduced SPED method into underwater acoustic broadband sonar signal

energy detection, and further proposed a beam domain detection. The experiment results show that its performance is limited by the resolutions of the original BTRs; Zheng et al. [8] combined SPED and image processing technology to extract the target trajectory of the BTR, while they did not solve the problem that the weak target at the intersection of the trajectory is covered; Jomon et al. [9] uses a combination of MVDR and SPED for detection and tracking of fast moving targets, and proposes an efficient parallel scheme; Luo et al. [10] used median filtering and order truncation averaging methods to estimate the background noise, and further determine the threshold value for peak judgment in the SPED algorithm, which can reduce the generation of false targets; Yang [11,12] used deconvolution algorithm in the underwater acoustic post-processing part, the main idea is to improve the quality of BTRs by computing its deconvolution with a point spread function (PSF); Zhao et al. [13] also applied the deconvolution algorithm to SPED to reduce the generation of many false targets on traditional spatial spectral estimation methods; Zhang et al. [14] proposed expanded-SPED algorithm improve cross-azimuth detection of weak targets under strong interference. Wang et al. [15] proposed a target localization algorithm based on 2-D SPED, which can achieve higher localization accuracy compared with bearing-only target localization.

Image processing methods have been used in passive sonar post-processing for several years. Li et al. [16] proposed using an image equilibrium method to smooth the background and improve the trajectory of the process map, but the improved trajectory would possess lower resolutions. Yin et al. [17] proposed a PCA algorithm to reduce noise on the noise-contaminated BTR. The noise reduction effect is good and the connection is also compensated at the break point of the trajectory due to the vertical singularity. In the field of pure natural image noise reduction, M. Aharon et al. [18] proposed the KSVD image noise reduction algorithm. As the natural images can be expressed sparsely whereas the noise cannot, the quality of the image can be easily improved with the help of some dictionary or primitive library. Antoni et al. [19] proposed a NLM algorithm for noise reduction by using the windowing method to superimposes the self-matched image blocks to enhance the interested information. K. Dabov et al. [20] proposed a noise reduction method based on 3D block matching, which provides a cleaner separation of noise and signal in a higher dimension with significant noise reduction effects. However, many algorithms (e.g., BM3D, KSVD) need to estimate the noise level of an image in order to obtain an a priori noise variance value to guide the subsequent more accurate noise reduction process. Currently, the commonly used image noise estimation algorithms are generally divided into three categories: (a). Smooth filter-based estimation [21,22], within which a noisy image is processed by various filtering methods, and the filtered image is treated as a clean image and the original noisy image is subtracted to obtain the difference, and then the noise is estimated. However, this smoothing filtering approach will blur the details and adversely damage the accuracy of the noise estimate in photos with many details and complicated high-frequency information. (b). The blocking-based approach [23,24], which divides the picture into image blocks based on predetermined criteria and chooses the smoother image blocks with lower variance for noise estimate. (c). Transform domain-based approaches [25,26], in which the original picture is converted into the frequency domain or wavelet domain for noise estimation, with high frequency diagonal subband noise estimation based on the wavelet domain being extensively employed.

In this paper, the BM-SEED algorithm is proposed for weak target enhancement and high bearing resolution. We choose CBF as the pre-process DOA algorithm, which is robust and has been widely used in underwater detection. Next, SEED algorithm is applied to enhance the target trajectories. In order to suppress the background noise caused by the peaking operation of multiple frequency points, we further use empirical mode decomposition (EMD) to extract the main frequency components of the signal. Considering that the false target is mainly composed of various random noise points, we finally introduce the BM3D algorithm for post-processing noise reduction and false target suppression. BM3D includes 3D transformation, Wiener filtering and collaborative

filtering steps. It filters the whole reference block instead of the reference center pixel point, which makes the computational rate of the whole algorithm improved and the noise reduction performance more obvious. Since it is a non-fully adaptive algorithm that requires a priori noise estimation to set the filtering threshold, and the noise estimation method mentioned above does not work well directly on the BTR after the improved SEED. Then, we propose a new noise estimation algorithm to estimate the noise values introduced by the improved SEED.

The main contributions of this paper includes:

- (a) The SEED algorithm is improved and incorporated into the proposed BTR post-processing framework, in order to address the problem that weak targets are easily obscured by strong sidelobe.
- (b) The BM3D algorithm is introduced to suppress background noise and false targets caused by SEED algorithm.
- (c) This paper proposes a BTR noise estimation method to provide the priori noise information for the noise reduction part, in order to improve the adaptivity of the proposed BTR enhancement method.

The reminder of this paper organized as follows: Section 2 elaborates the proposed BM-SEED algorithm; Section 3 evaluates the proposed method via simulations and sea trial data; Section 4 discusses the findings of this work and a conclusion is given.

2. Proposed Method

In this section, we propose the BM-SEED algorithm to enhance weak targets and reduce the influence of background noise. As shown in Figure 1, the recommended algorithm involves three parts: (a) the peak features of the BTR via the improved SEED algorithm eliminate energy differences between strong and weak target trajectories; (b) the peak feature map is filtered adaptively via a user-defined hard threshold to eliminate random noise; (c) the peak feature maps are further filtered via empirical Wiener filter based on the matching-block.

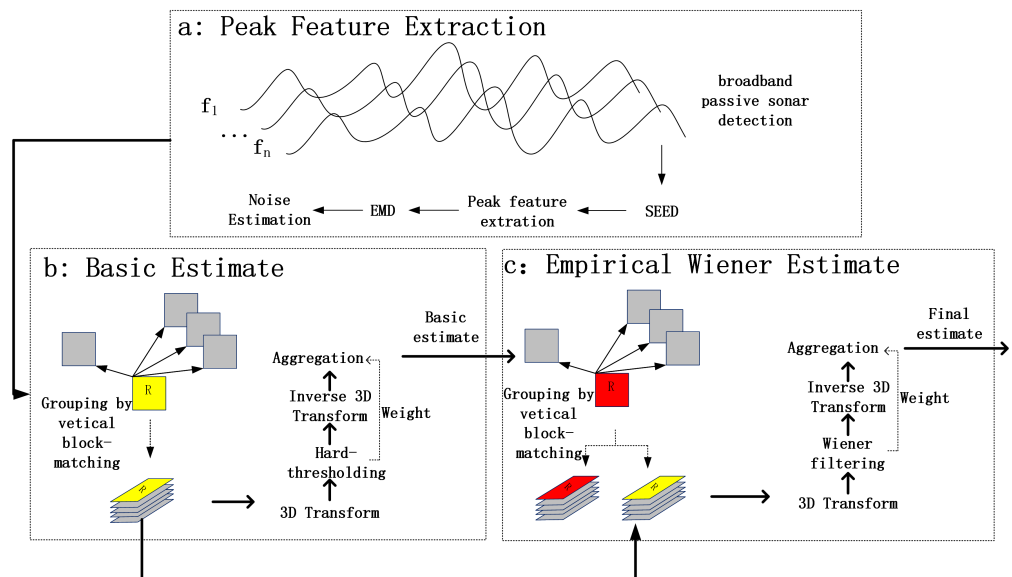


Figure 1. Frame of proposed method.

2.1. Peak Feature Extraction

As shown in Figure 1a, this paper selects and improves the SEED algorithm to extract the peak feature of the original BTRs, which can enhance the energy of weak targets, and the improved SEED method can be described as follows:

$$z(\theta) = y(\theta) + n(\theta) \tag{1}$$

where θ is the scanning bearing, $z(\theta)$ is one snapshot of the extracted peak feature map, $y(\theta)$ is one snapshot of the clean BTR map, and $n(\theta)$ is the independent identically distributed random noise and interference. We assume that $n(\theta)$ follows a statistical distribution with mean $E(\theta)$ and variance $D(\theta)$, respectively. The mean of $y(\theta)$ is $E(\theta)$ and the variance is 0, so $z(\theta)$ follows some statistical distribution $P(E(\theta) + E(\theta), D(\theta))$.

For the purpose of denoising, we adaptively analyze the input signal and incorporate EMD to extract the signal reflecting the lowest frequency component. The noise estimation algorithm described in Algorithm 1 is applied in Figure 1a to provide prior information for subsequent denoising implementation. The difference map are chunked into $N * N$ blocks, then average their covariance matrices [27]. Next, the covariance matrix, whose size is $N^2 \times N^2$, is decomposed by SVD and the singular values are sorted in descending order. Finally, the noise level is estimated as

$$A = U \times S \times V^T \tag{2}$$

where A is a matrix of order $m * n$ of rank r , U and V are singular vectors of A , and S is the singular value of A , which is a diagonal matrix. Among them, U is $m \times m$ square matrix, $U^T * U = I_{mm}$, U is $m \times m$ square matrix, $V^T * V = I_{nn}$.

In empirical estimation, the BTRs are considered to be made up entirely of noise, so the mean of the larger singular values represents the noise value level. The experimental results show that the first singular value is much larger than the others, but since it contains a weak target energy enhancement that was deliberately introduced earlier, so the average of the first two singularities is used as the noise sigma level.

$$\sigma^2 = \frac{1}{2} \sum_{i=1}^2 s_n^2(i) \tag{3}$$

where σ is noise level estimate, $s(i)$ is the i -th singular value.

Since the level of the first singular is much larger than the latter one, it takes into account the main energy values in the differential BTR and avoids attenuating the energy enhancement of the weak BTR targets.

Algorithm 1: Noise Estimation.

Input: Difference matrix of raw BTR and SEED processing results

- a. Take block operation, the block size is $N * N$ and the step size is 1;
- b. Sum all the blocks and calculate the final mean block;
- c. Calculate the covariance matrix for all blocks, the size is $N^2 * N^2$;
- d. Find the singular value of the covariance matrix, the size is $N^2 * N^2$;
- e. Arrange the singular values in descending order, and find the mean τ of the first two singular values;

return Noise estimated value $\sigma = \sqrt{\tau}$.

2.2. Hard Threshold filtering

As shown in Figures 1b and 2, we use hard threshold filtering to reduce background noise and false targets. The peak feature map of the input BTR is filtered adaptively, which is constructed via block matching. More precisely, each pixel's neighborhood is utilized as a reference block. In order to reduce the computational complexity, it starts with the first $N_1 \times N_1$ block of the BTR and uses a raster scan, which pans a few columns (rows) at a time (denoted for example by $N_{step} < N_1$), until the whole BTR or region of interest (ROI) is covered. As we must ensure that all pixels participate in collaborative filtering at least once, all blocks are selected as reference blocks once, and the overlapping of reference blocks is also a manifestation of overcompleteness.

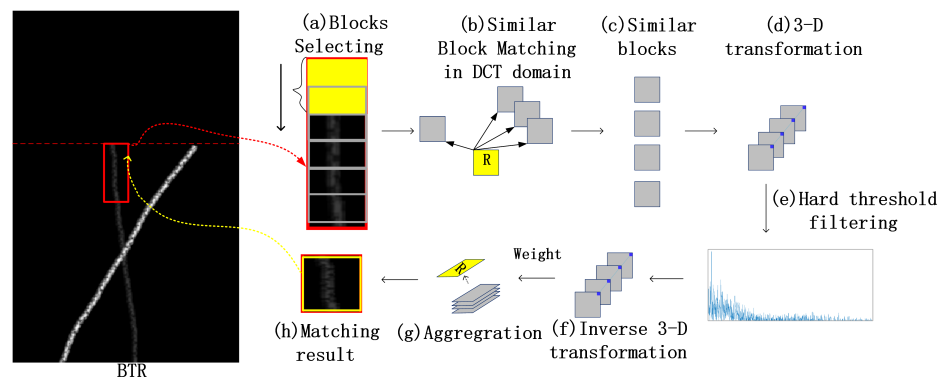


Figure 2. Frame of hard threshold filter.

According to the self-coherence of the BTR target trajectory, we design a search window for each reference block as shown in Figure 2a, and extends along the time axis. In this way, for the latest N_1 snapshots data, the previously accumulated detection information can be used to enhance the relevant target trajectory via a matching procedure. For a noiseless BTR y , the matching error or block distance d^{idel} between the reference block Y_{xR} and the block Y_x is noted as

$$d^{idel}(Y_{xR}, Y_x) = \frac{\|Y_{xR} - Y_x\|_2^2}{(N_1^{ht})^2} \tag{4}$$

where $\|\cdot\|_2^2$ is the square of the Euclidean norm, and N_1^{ht} is width/height of Y_{xR} . If the two blocks do not overlap, i.e., each pixel is independent, then [20] points out that the mathematical expectation and variance of the matching error of the two blocks at the corresponding positions on the noisy BTR $z(x)$ are

$$E[d^{noisy}(Z_{xR}, Z_x)] = d^{idel}(Y_{xR}, Y_x) + 2\sigma^2, \tag{5}$$

$$D[d^{noisy}(Z_{xR}, Z_x)] = \frac{8\sigma^4}{(N_1^{ht})^2} + \frac{8\sigma^2 d^{idel}(Y_{xR}, Y_x)}{(N_1^{ht})^2}. \tag{6}$$

where σ is the estimated noise variance. When the noise variance is large or the blocks are relatively small, the matching error between the blocks is large as shown in Equation (6), so it is not accurate to look for similar blocks directly on the noisy BTR z , and two blocks with a large difference on the noiseless BTR y may be similar on the noisy image z due to the large variance, resulting in an incorrect match. To solve this problem, the two blocks on the noisy image z are first subjected to a two-dimensional Discrete Cosine Transform (DCT) as shown in Figure 2b, and then those coefficients whose magnitude is less than a certain threshold are set to zero, so that the matching error of the two blocks can be expressed as the mean square error of these coefficients [20], that is

$$d(Z_{xR}, Z_x) = \frac{\|Y'(\Gamma_{2D}^{ht}(Z_{xR})) - Y'(\Gamma_{2D}^{ht}(Z_x))\|_2^2}{(N_1^{ht})^2} \tag{7}$$

where Y' represents the hard thresholding operation and the corresponding threshold represents $\lambda_{2D\sigma}$, typically 2 to 3 standard deviations (empirical values for image processing). Γ_{2D}^{ht} computes the corresponding two-dimensional DCT. The high-frequency random noise will be retained after the orthogonal transform, while the noiseless BTR generally only has larger values at a few low-frequency locations due to its sparsity in the transform domain. Hence, we can remove most of the noise energy by setting the hard threshold after the 2D orthogonal transform.

Furthermore, since we have already calculated the 2D transform coefficients of all similar blocks as shown in Figure 2c, if the collaborative transform uses a separable 3D

orthogonal transform, the results of these 2D transforms can be reused, and we only need to perform a 1D transformation of the third dimension to further reduce its complexity. In terms of block matching, we only maintain those blocks whose error is less than a specific threshold after computing the matching error, and then obtain the corresponding coordinate set

$$S_{xR}^{ht} = x \in X : d(Z_{xR}, Z_x) \leq \tau_{match}^{ht} \tag{8}$$

where S_{xR}^{ht} represents the coordinate set of similar blocks for corresponding reference block, x represents a single pixel, X represents the ROI on BTR, $d(Z_{xR}, Z_x)$ is the distance between reference block Z_{xR} and block Z_x in corresponding vertical window, τ_{match}^{ht} is an empirically determined maximum error threshold for identifying the similarity of two blocks. Obviously, the present reference block itself will be evaluated as a comparable block as its matching error is 0, indicating that there is at least one element in the coordinate set. Then we stack all comparable blocks to create a 3D array $Z_{S_{xR}^{ht}}$ with the shape $N_1^{ht} \times N_1^{ht} \times |S_{xR}^{ht}|$ as shown in Figure 2d, where $|S_{xR}^{ht}|$ represents the number of items in the set. The components in the third dimension are sorted in ascending order based on the matching error. Then, we can execute 3D collaborative transformation and filtering after acquiring the 3D array corresponding to the reference block, which can be formally described as

$$\hat{Y}_{S_{xR}^{ht}}^{ht} = \Gamma_{3D}^{ht-1}(\Upsilon(\Gamma_{3D}^{ht}(Z_{S_{xR}^{ht}}))) \tag{9}$$

where Γ_{3D}^{ht} represents the corresponding 3D orthogonal transformation. Generally speaking, we will use a separable transformation to decrease the complexity of the computation since the results of the preceding two-dimensional transform are already available for reuses when computing the block matching error. Therefore, Γ_{3D}^{ht} can be expressed as a combination of Γ_{2D}^{ht} in the first two dimensions and Γ_{1D}^{ht} in the third dimension. The transform in the first two dimensions is chosen to be of the Fourier transform type such as DCT, which can better capture the periodic information in the BTR block, and the third-dimensional transformation uses the wavelet transform type such as Haar wavelet, which better captures the local similarity between blocks by scaling. Υ represents another hard threshold operation, and the corresponding threshold is $\lambda_{3D\sigma}$, usually takes 2 to 3 standard deviations empirically. $\hat{Y}_{S_{xR}^{ht}}^{ht}$ contains $|S_{xR}^{ht}|$ blocks $\hat{Y}_x^{ht,xR}$, representing the result of collaborative filtering by Equation (9), corresponding to a reference block with coordinates x_R . As different reference blocks may contain similar blocks, a block will also correspond to multiple collaborative filtering results. Therefore, it is necessary to distinguish by using its corresponding reference block coordinates, and these different filtering results will be integrated in the later operations to obtain the basic estimate for each pixel.

Since the different reference blocks may also contain similar blocks that overlapped, it is necessary to integrate these collaborative filtering results from different combinations to obtain the basic estimate of each pixel after obtaining the collaborative filtering results of each reference block and its corresponding 3D group.

As a result, we allocate the weights based on the number of non-zero coefficients. Assuming that all pixels in the 3D combination are independent and that the number of coefficients left after the hard threshold operation as shown in Figure 2e is N_{hard}^{xR} , we obtain

$$\omega_{xR}^{ht} = \begin{cases} \frac{1}{\sigma^2 N_{hard}^{xR}} & \text{if } N_{hard}^{xR} \geq 1 \\ 1 & \text{otherwise} \end{cases} \tag{10}$$

In actuality, similar blocks inside a 3D combination may frequently overlap, implying that all pixels are not fully independent of one other, but for convenience, we shall calculate the weights using Equation (10). In order to reduce boundary effects, the Kaiser window is used for each block to provide a larger weight to the central pixel.

Finally, we generate its base estimate by superimposing the weights of all the reference blocks to which a pixel belongs and the corresponding similar blocks as shown in Figure 2f,g,

i.e., each reference block and its similar blocks will be added to the initial location of the reference block in a weighted way [20] as follows:

$$\hat{y}^{basic}(x) = \frac{\sum_{xR \in X} \sum_{x_m \in S_{xR}^{ht}} \omega_{xR}^{ht} \hat{Y}_{x_m}^{ht, xR}(x)}{\sum_{xR \in X} \sum_{x_m \in S_{xR}^{ht}} \omega_{xR}^{ht} \chi_{x_m}(x)}, \forall x \in X \tag{11}$$

where we assume that each block has been filled with zeros to the same size as the original BTR, and determine whether a pixel x is on block x_m by $\chi_{x_m} : X \rightarrow \{0, 1\}$ (for normalization of the weights summation).

2.3. Empirical Wiener Shrinkage

In this subsection, we employ the empirical Wiener shrinkage technique as shown in Figures 1c and 3 for higher detection gains, which is based on the principle of estimate the power spectrum of the transform coefficients on the basic estimated BTR in order to shrink the transform coefficients of the original noisy BTR.

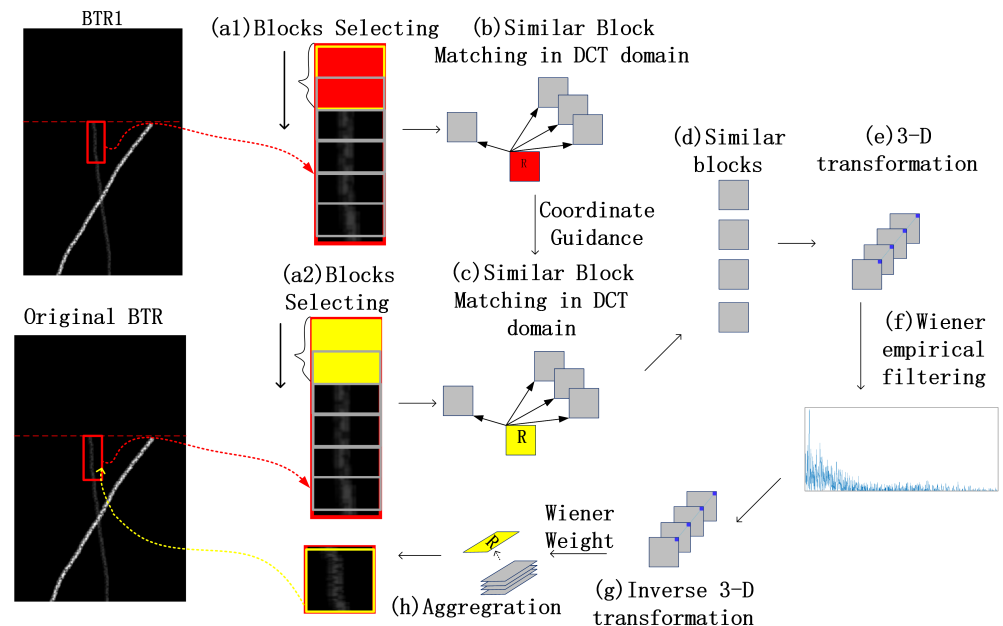


Figure 3. Frame of Wiener empirical shrinkage.

As shown in Figure 3(a1,a2), enough similar blocks for each reference block are found out in a vertical window

$$S_{xR}^{wie} = \{x \in X : \frac{\|\hat{Y}_{xR}^{basic} - \hat{Y}_x^{basic}\|_2^2}{(N_1^{wie})^2} \leq \tau_{match}^{wie}\} \tag{12}$$

where S_{xR}^{wie} represents the coordinate set of similar blocks for corresponding reference block, x represents a single pixel, X represents the ROI on BTR, \hat{Y}_{xR}^{basic} represents reference block on basic estimated BTR obtained in the last step, $\|\hat{Y}_x^{basic} - \hat{Y}_{xR}^{basic}\|_2^2$ represents the block distance between \hat{Y}_x^{basic} and reference block $\hat{Y}_{xR}^{basic} - \hat{Y}$, $(N_1^{wie})^2$ represents block size, and τ_{match}^{wie} represents an empirically determined maximum error threshold.

Now two 3D combinations are generated, namely $\hat{Y}_{S_{xR}^{wie}}^{basic}$ and $Z_{S_{xR}^{wie}}$. This is a 3D combination of similar blocks on the basic estimated BTR as shown in Figure 3b, and the latter is the original noisy BTR block in the same position as shown in Figure 3c. The Wiener filter is a linear filter that minimizes the mean square error between the filtered output

of the noisy signal and the original noise-free signal. Its discussion is generally in the frequency domain, a commonly used definition is

$$H(u, v) = \frac{H_d^*(u, v)}{|H_d(u, v)|^2 + \frac{P_n(u, v)}{P_s(u, v)}} \tag{13}$$

where $H(u, v)$ represents the frequency response function of the Wiener filter and $H_d^*(u, v)$ is the frequency response function of the degenerate system. $P_n(u, v)$ and $P_s(u, v)$ represent the power spectrum of the noise and the original signal, respectively.

Specifically, we use T_y to denote the transform coefficient of the noiseless BTR and T_z the transform coefficient of the corresponding noisy BTR, then it has

$$T_z(x) = T_y(x) + \eta(x), \eta(x) \sim P(E(\eta(x)), \sigma^2) \tag{14}$$

The mathematical expectation of the power spectrum of the noisy and noisy BTR can be found as

$$E(\eta^2(x)) = D(\eta(x)) + E^2(\eta(x)) = E^2(\eta(x)) + \sigma^2, \tag{15}$$

$$E(T_z^2(x)) = E((T_y(x) + \eta(x))^2) = T_y^2(x) + 2T_y(x)E(\eta(x)) + E^2(\eta(x)) + \sigma^2. \tag{16}$$

Since we have repeatedly mentioned that the basic estimated BTR can be used as an empirical estimate of the original noiseless BTR, the spectrum T_y of the noiseless BTR can be replaced by the spectrum of the basic estimated BTR. Substituting the empirical estimates of the basic estimated BTR and the power spectrum of the noise into Equation (13) yields

$$H(x) = \frac{1}{1 + \frac{P_n(x)}{P_s(x)}} = \frac{P_s(x)}{P_s(x) + P_n(x)} = \frac{T_{ybasic}^2(x)}{T_{ybasic}^2(x) + \sigma^2} \tag{17}$$

where $T_{ybasic}^2(x)$ is the basic estimate BTR, σ^2 is the power spectrum of the noise. Then an intuitive filtering method can be defined as a classical Wiener filter expression

$$T'_Z(x) = \frac{T_{ybasic}^2(x)}{T_{ybasic}^2(x) + \sigma^2} T_Z(x) \tag{18}$$

where $T_Z(x)$ is the transform coefficient of the corresponding noisy BTR, $T'_Z(x)$ is the transform coefficient after empirical Wiener filter. After the hard threshold filtering in the previous step, the noise reduction BTR no longer has so much impulsive noise, i.e., the Wiener filter is more suitable for the second step of noise reduction, which is less effective if it directly deals with too much impulsive noise.

Since the Wiener filter is a linear filter with the optimal mean square error, the result of Equation (18) is mathematically expected to minimize the mean square error of the output BTR with respect to the original noise-free signal. After obtaining the basic estimated BTR and the two 3D combinations \mathbf{Y}_{xR}^{basic} and \mathbf{Z}_{xR}^{basic} at the same position on the original noisy BTR respectively, we can obtain

$$\mathbf{Y}_{xR}^{wie} = \Gamma_{3D}^{wie-1}(\mathbf{W}_{xR}^{wie} \times \Gamma_{3D}^{wie-1}(\mathbf{Z}_{xR}^{wie})) \tag{19}$$

where $\mathbf{W}_{xR}^{wie} = \frac{|\Gamma_{3D}^{wie}(\mathbf{Y}_{xR}^{basic})|^2}{|\Gamma_{3D}^{wie}(\mathbf{Y}_{xR}^{basic})|^2 + \sigma^2}$, $|\cdot|$ represents the modulus of a complex number, \mathbf{W}_{xR}^{wie} is the coefficient matrix after Wiener filtering. Wiener shrinkage can not only suppress part of the noise energy, but also preserve the detailed information of the BTR itself. Therefore,

compared to the hard threshold filtering of Step 2, Step 3 can reduce noise in all frequency bands without losing the high frequency.

Assuming that all pixels in the 3D combination are independent, the residual noise is proportional to the second-order norm of the shrinkage coefficient matrix, so similar to Equation (10), the weight that defines the combination as [20] is

$$\omega_{xR}^{wie} = \sigma^{-2} \|\mathbf{W}_{S_{xR}^{wie}}\|_2^{-2} \tag{20}$$

where $\mathbf{W}_{S_{xR}^{wie}}$ is the coefficient matrix after Wiener filtering.

Likewise, we can add a Kaiser window to give more weight to the pixels in the center of the block as shown in Figure 3g,h, thereby reducing edge effects. Then, similar to Equation (11), the final estimated BTR obtained in Step 3 can be expressed as

$$\hat{y}^{final}(x) = \frac{\sum_{xR \in X} \sum_{xm \in S_{xR}^{wie}} \omega_{xR}^{wie} \hat{Y}_{xm}^{wie,xR}(x)}{\sum_{xR \in X} \sum_{xm \in S_{xR}^{wie}} \omega_{xR}^{wie} \chi_{xm}(x)}, \forall x \in X \tag{21}$$

where we assume that each block has been filled with zeros to the same size as the original BTR, and determine whether a pixel x is on block x_m by $\chi_{xm} : X \rightarrow \{0, 1\}$.

Although Steps 3 and 2 both directly denoise the original noisy BTR, Step 3 additionally employs the basic estimated BTR acquired in Step 2. Furthermore, it can precisely locate related blocks, and on the other hand, it can be utilized as an empirical estimate of the original noise-free BTR to conduct Wiener filtering with optimum mean square error.

3. Simulations

In this section, we experimentally validated the technique in multi-target jamming and low SNR situations in the following simulations, respectively. The frequency range of the simulated ship radiation noise signal is 100 Hz~1000 Hz, and the sampling frequency is 4000 Hz. The receiving array is a 64-units horizontal linear sonar array, with a spacing of 0.75 m between the array unit. The measuring signal angle ranges from 0 to 180 degrees, with a precision of 0.5 degrees.

3.1. Jamming-Targets

This subsection evaluates the detection capability of the proposed method within a jamming-targets environment. As shown in Figure 4a, we have simulated a total of 30 snapshots of array-received data, there is a slow moving strong target at 90 degree, and the angle has nearly no change within 30 snapshots. Then we set the Signal-to-Interference ratio (SIR) of a weak target to -20 dB, the background SNR to 0 dB, and move rapidly from an angle of 60 degree to 120 degree. The weak target trajectory can hardly be detected via naked eyes.

We choose the deconvolution algorithm as the baseline of the experiment. The core of the deconvolution algorithm is that the DOA spectra are obtained by convolving the real energy distribution of the target in space with the PSF function, while the PSF function can be calculated from the known array information, and then the real target energy distribution can be calculated by the inverse operation. Figure 4b depicts the experimental findings, the mainlobe of the strong target has been significantly narrowed, and the target trajectory's resolution has been improved. However, the energy of the weak target trajectory has not been improved, and it is still difficult to see clearly compared to Figure 4a, and it even has a weakening effect on weak targets.

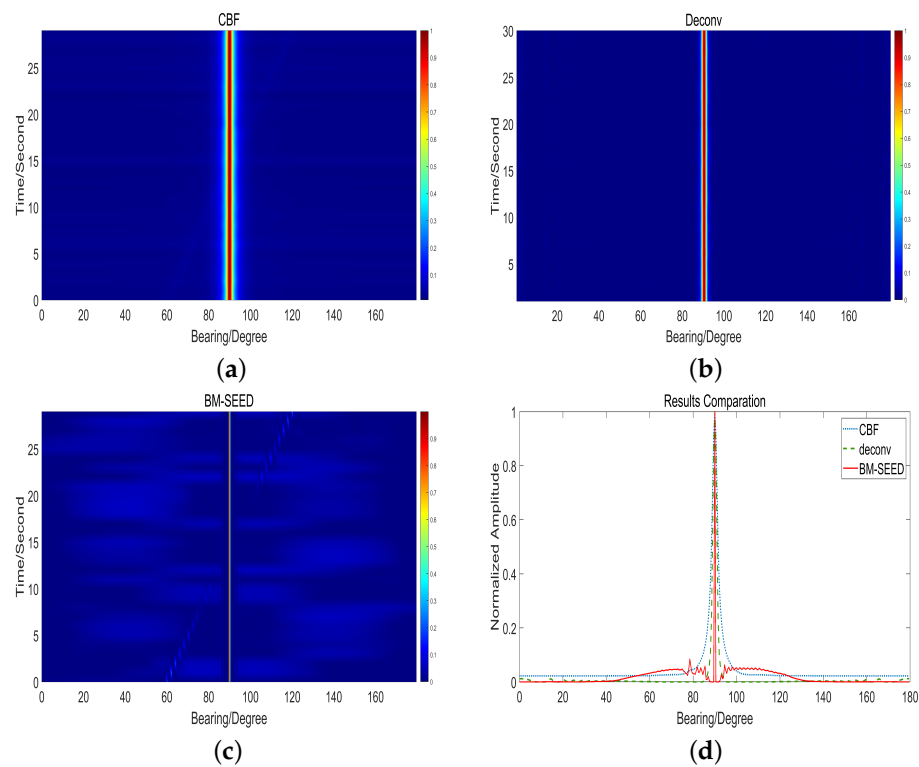


Figure 4. Experiment Results under -20 dB SIR; (a) CBF result under -20 dB SIR; (b) Deconv result under -20 dB SIR; (c) BM-SEED result under -20 dB SIR; (d) Results-Comparison under -20 dB SIR.

The processing outcome of the approach provided in this work is shown in Figure 4c and Table 1. The mainlobe width is more than 2 degrees lower than that of the deconvolution algorithm, and the fast-moving weak target trajectory is also much improved.

Table 1. Beamwidth (degree) under different SIR .

SIR (dB)	CBF	Deconvolution	BM-SEED
-20	6.8 degree	3.2 degree	1 degree
-25	7.1 degree	3.5 degree	1.1 degree

In order to compare the differences between the proposed method and other algorithms in more detail, we extract the middle moment snapshots of the above three results (which can avoid the influence of the first and last moments on the waveform stability). Figure 4d shows the comparison result that the proposed approach’s mainlobe width is almost 1.0 degree, the CBF and deconvolution’s mainlobe width are almost 6.8 and 3.2 degree, respectively, and the weak target is enhanced as well. This demonstrates that the proposed approach in this study not only dramatically narrows the width of the mainlobe, but also has a favorable effect on enhancement of weak targets.

Finally, we further reduce SIR down to -25 dB, the experimental findings are given in Figure 5a–c, where it can be observed that the mainlobe width of target is still almost decreased to 1.1 degree, and weak targets have a certain improvement impact. To further understand the algorithm’s performance, we took the middle snapshot data, as shown in Figure 5d. The mainlobe width of the target is obviously narrowed, but the enhancement of the weak target near 79 degrees is not obvious enough. It can also be seen in the BTR Figure 5c that the trajectory improvement is not as good as the previous set of experiments. That is, the enhancement effect has reached the limit of algorithm performance.

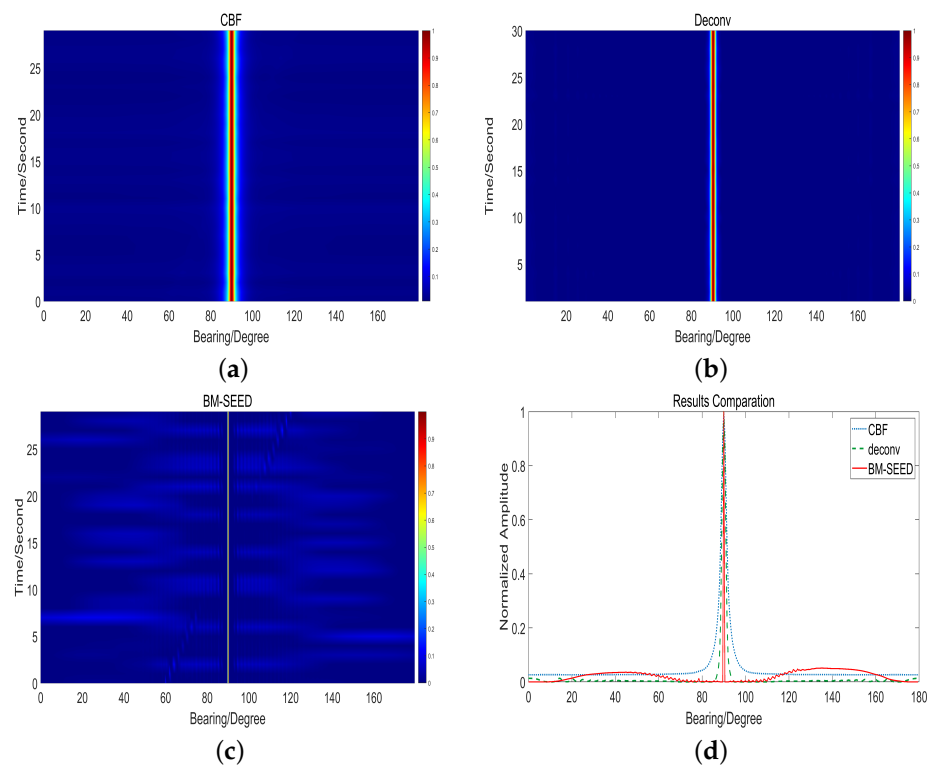


Figure 5. Experiment Results under -25 dB SIR. (a) CBF result under -25 dB SIR; (b) Deconv result under -25 dB SIR; (c) BM-SEED result under -25 dB SIR; (d) Results-Comparison under -25 dB SIR.

3.2. Low-SNR Environments

This subsection evaluates the performance of the proposed method within different SNR environments. The noise used in this experiment is in-band Gaussian white noise that has been time-domain filtered to 100–1000 Hz to eliminate superfluous noise outside the frequency region. First, a set of experiments is required to add noise to SNR = -20 dB. The target moves at a constant speed from 30 degrees to 40 degrees, and CBF is used for beamforming. The obtained BTR is shown in Figure 6a, it can be seen that the target trajectory formed by traditional CBF is very wide, and the background noise has a certain interference effect on the target trajectory. Then we use the deconvolution and proposed method to process the BTR in the post-processing stage, respectively.

The experiment results are shown in Figure 6b and Figure 6c, respectively. Figure 6d shows the single snapshot comparison. With energy magnitude normalization, it can be seen that the background noise magnitude of CBF is around 0.7, the deconvolution algorithm results in around 0.4, while the background noise of the proposed method has reached 0.2, which is less than the others. Moreover, the proposed method’s noise floor is smoother, which will be better for target tracking.

The performance of the algorithm is further investigated at SNR = -25 dB. The experimental results are shown in Figure 7a–c. The single snapshot is depicted in the Figure 7d, and the comparison demonstrates that the CBF’s background noise level is almost 0.8, the deconvolution’s result is around 0.6, and the proposed method’s noise floor is greatly decreased to almost 0.35, demonstrating that the proposed method still performs well under such situation. Then reduce the signal-to-noise ratio to -26 dB as shown in Figure 8a, the processed BTR as shown in Figure 8b, the background noise is still greatly reduced, but the trajectory changes at the beginning and end of the target trajectory. Then the target trajectory processed by CBF, deconvolution, and the proposed method is used for tracking processing. The mean square error (MSE) of the tracking results is shown in Figure 9, and the track accuracy obtained are 2.147, 1.602, and 0.996 degrees. That is, the tracking accuracy of the proposed method can still be kept within 1 degree under the signal-to-noise

ratio of -26 dB, and lower SNR will induce drift of the target trajectory in post-processing due to noise damage to the original trajectory.

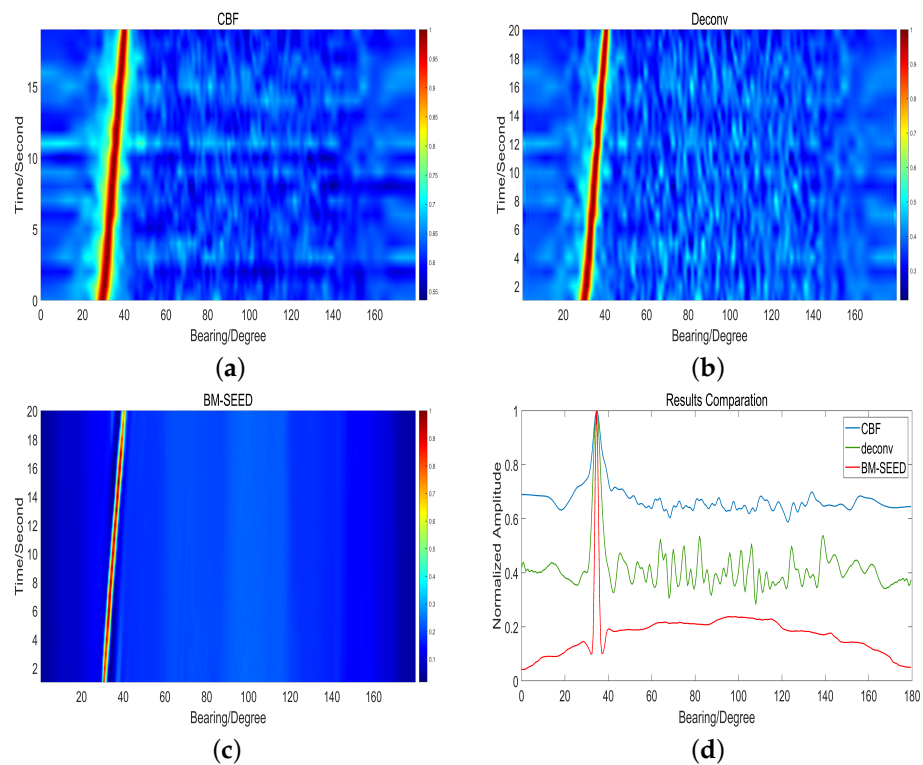


Figure 6. Experiment Results under -20 dB SNR. (a) CBF result under -20 dB SNR; (b) Deconv result under -20 dB SNR; (c) BM-SEED result under -20 dB SNR; (d) Results-Comparasion under -20 dB SNR.

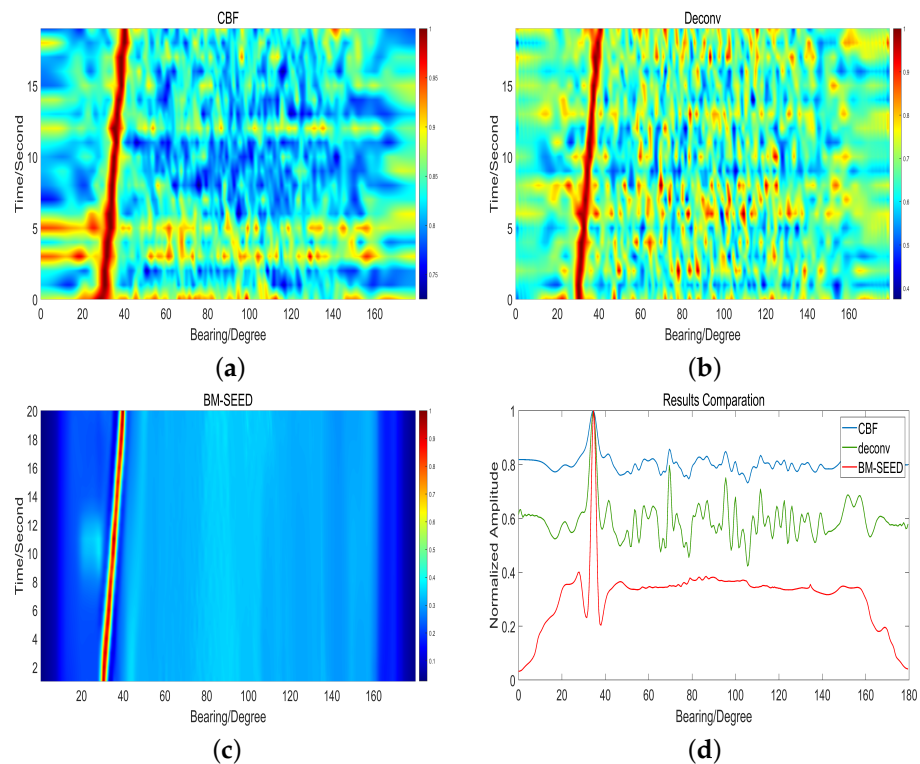


Figure 7. Experiment Results under -25 dB SNR. (a) CBF result under -25 dB SNR; (b) Deconv result under -25 dB SNR; (c) BM-SEED result under -25 dB SNR; (d) Results-Comparasion under -25 dB SNR.

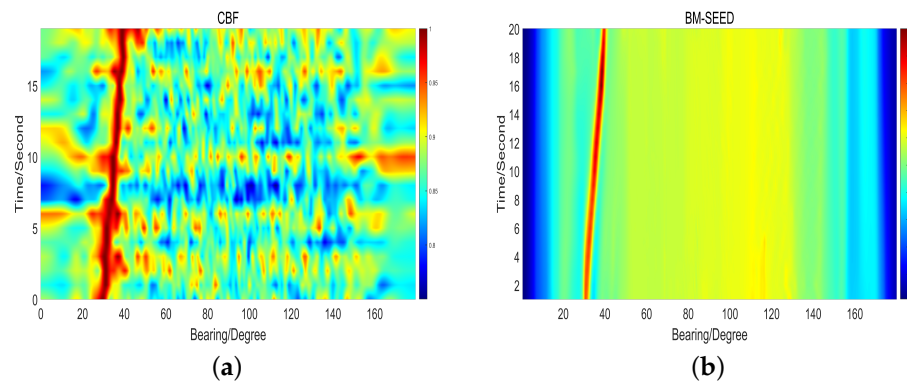


Figure 8. Experiment Results under -26 dB SNR. (a) CBF result under -26 dB SNR; (b) BM-SEED result under -26 dB SNR.

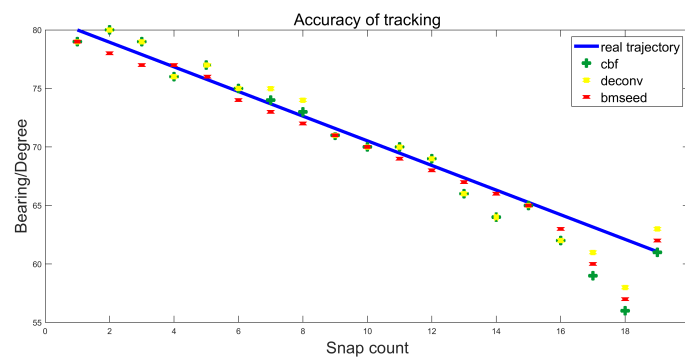


Figure 9. Accuracy of tracking results.

4. Sea-Trial Experiments

The experiments of this section evaluate the BM-SEED method by using sea-trial data, and the data are collected in the South China Sea, in the summer of 2021. The sonar array utilized in the experiment is a towed horizontal line array with 256 elements, the unit distance is 1.5 meters and the frequency band of the detection signal is 250–400 Hz.

As shown in Figure 10a, there are two strong targets at 60 degree and 100 degree respectively, and there are weak target tracks near 75 degree. We use the traditional SEED algorithm to obtain the processing result as shown in Figure 10b and the trajectory resolution is improved, but the weak target enhancement is not good, and many interference false weak targets appear in the background. Then we use the improved SEED algorithm as shown in Figure 11a, the weak target is enhanced but the false target is enhanced as well, and the resolution is also improved as shown in Figure 11b after using the deconvolution method, but the weak target energy is suppressed. Finally, we use the method proposed in this paper, the overall resolution is greatly improved, and an obvious target track appears near 75 degree and 115 degree as shown in Figure 11c, which is not seen in the deconvolution BTR at all. These experiment results show the good performance for weak target enhancement by using the proposed method. Then as shown in Figure 11d, some targets with weak energy are enhanced greatly by the proposed algorithm compared with the other two algorithms.

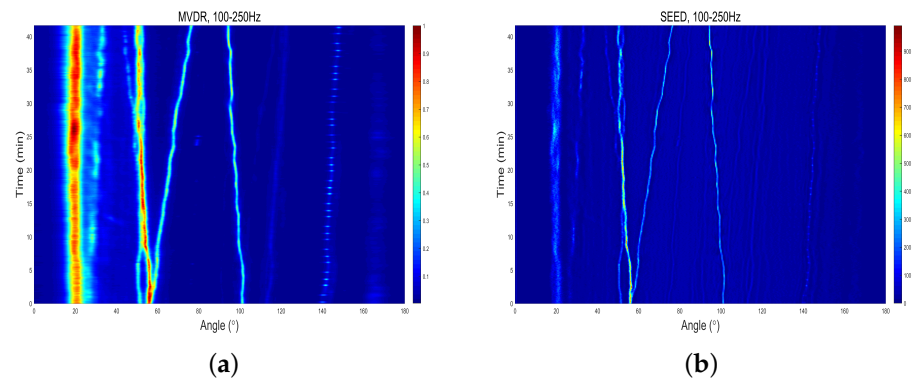


Figure 10. Sea-trial experiments. (a) Original MVDR1; (b) SEED.

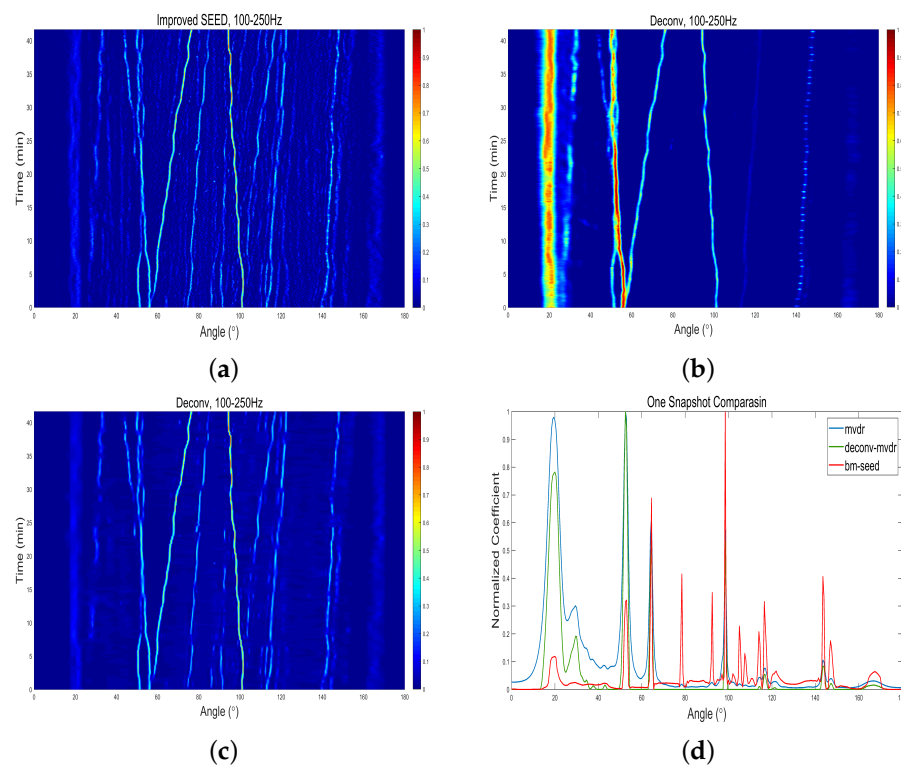


Figure 11. Sea-trial experiments 2. (a) improved SEED; (b) Deconv MVDR1; (c) BM-SEED MVDR1; (d) Snapshot Comparison.

Then we choose other experiment data as shown in Figure 12a to verify the proposed method, the original BTR of this experiment is based on the MVDR algorithm. The resolution of Figure 12b can be improved after deconvolution, but at 80 degrees, several weak target tracks at 30 min are weakened. As shown in Figure 12c, the resolution is not only improved, but also the trajectories strength of several weak targets at the same position are improved. Finally, as shown in Figure 12d, the BM-SEED algorithm can apparently enhance the weak targets in DOA spectrum.

The proposed algorithm reduces the trajectory energy difference between the weak targets and the strong interference targets, resulting in an improved weak targets after normalization. Some of the pseudo-targets experience energy enhancement during the peak feature extraction, but due to the randomness of the presence of pseudo-targets, it is difficult to form regular and effective trajectories on the BTR, which will be considered as impact noise and smoothed out by the proposed algorithm, i.e., the proposed algorithm can simultaneously reduce the background noise and the presence of pseudo-targets at the same time. The aforesaid experimental effect is more visible in single-tap trials. The findings

reveal that the BM-SEED algorithm performs well in four aspects: noise suppression, high resolution, weak target enhancement, and low SNR detection capabilities.

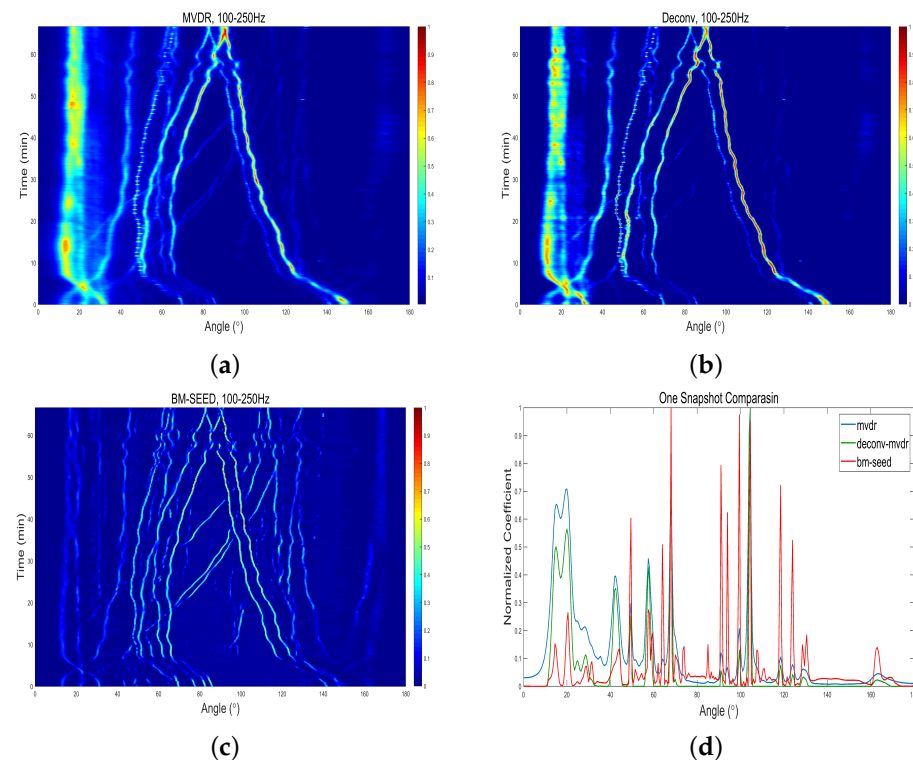


Figure 12. Sea-trial experiments 2. (a) Original MVDR2; (b) Deconv MVDR2; (c) BM-SEED MVDR2; (d) Snapshot Comparison.

5. Conclusions

This paper proposes a BM-SEED algorithm for the post-processing of underwater acoustic detections, which includes peak feature extraction, hard threshold filtering and empirical Wiener shrinkage.

The proposed BM-SEED algorithm not only has a very outstanding ability in improving the resolution, but also has excellent performance in enhancing the trajectory of weak targets. In addition, we further consider the performance of the algorithm under low SNRs, and experiments show that it still works well under low SNR. Finally, we use the actual sea trial data to verify the algorithm. It can be observed that the proposed algorithm is still significantly better than the deconvolution algorithm in terms of resolution improvement and weak target enhancement, which is consistent with the simulation results. However, in the case of more complex noise background such as deep-sea hydroacoustic environment, the method is difficult to completely remove the influence of noise, and may introduce false signals, bringing detection errors to the sonar system. Therefore, in the actual sea trial data, the method is more applicable to the BTR obtained from shallow sea environment. Moreover, in the follow-up algorithm research, we will further use GPU parallel computing to improve the real-time running performance of the algorithm.

Author Contributions: F.Y. (Fan Yin): Methodology, software, methodology, writing, investigation, writing—original draft preparation; C.L. (Chao Li): Investigation, resources, data curation, project administration and funding acquisition; H.W.: Investigation, resources, writing—review and editing, supervision, project administration and funding acquisition; L.N.: Investigation, conceptualization, writing—review and editing; Y.Z.: Investigation, conceptualization, writing—review and editing; C.L. (Chaonan Liu): Investigation, data curation; F.Y. (Fan Yang): Investigation, conceptualization, writing—review and editing. All authors have read and agreed to the published version of the manuscript.

Funding: This research was supported by the National Natural Science Foundation of China (ID:62171440) and China Scholarship Council, Chinese Academy of Sciences.

Institutional Review Board Statement: Not applicable.

Informed Consent Statement: Not applicable.

Data Availability Statement: No new data were created or analyzed in this study. Data sharing is not applicable to this article.

Acknowledgments: The authors would like to thank the editors and reviewers for their comments on the manuscript of this article.

Conflicts of Interest: The authors declare that they have no competing interest.

Abbreviations

The following abbreviations are used in this manuscript:

BTR	Bearing time record
BM-SEED	Block Matching - Subband Extrema Energy Detection
CBF	Conventional beamforming
SPED	Sub-band peak energy detection
DOA	Directions estimating of arrivals
SNR	Signal-to-noise ratio
SED	Subband energy detection
SEED	Subband Extrema Energy Detection
PSF	Point spread function
EMD	Empirical mode decomposition
ROI	Region of interest
DCT	Discrete Cosine Transform

References

- Bartlett, M.S. Smoothing periodograms from time-series with continuous spectra. *Nature* **1948**, *161*, 686–687. [\[CrossRef\]](#)
- Bartlett, M.S. Periodogram analysis and continuous spectra. *Biometrika* **1950**, *37*, 1–16. [\[CrossRef\]](#)
- Capon, J. High-resolution frequency-wavenumber spectrum analysis. *Proc. IEEE* **1969**, *57*, 1408–1418. [\[CrossRef\]](#)
- Schmidt, R.O. *A Signal Subspace Approach to Multiple Emitter Location and Spectral Estimation*; Stanford University: Stanford, CA, USA, 1982.
- Roy, R.; Kailath, T. ESPRIT-estimation of signal parameters via rotational invariance techniques. *IEEE Trans. Acoust. Speech Signal Process.* **1989**, *37*, 984–995. [\[CrossRef\]](#)
- Bono, M.; Shapo, B.; McCarty, P.; Bethel, R. *Subband Energy Detection in Passive Array Processing*; Report; Texas Univ at Austin Applied Research Labs: Austin, TX, USA, 2000.
- Yixin, Y. Peak energy detection with application to passive sonar display. *Appl. Acoust.* **2003**, *5*, 31–35.
- Zheng, Y.; Hu, C.; Li, Q.; Sun, C. A real-time extraction method of multi-target bearing history. *J. Acoust.* **2005**, *1*, 83–88.
- Jomon, G.; Jojish, J.V.; Santhanakrishnan, T. MVDR Beamformer with Subband Peak Energy Detector for Detection and Tracking of Fast Moving Underwater Targets Using Towed Array Sonars. *Acta Acust. United Acust.* **2019**, *105*, 220–225. [\[CrossRef\]](#)
- Lou, W.; Fu, Q.; Feng, K. An Improved Method of Sub-band Peak Energy Detection. *J. Phys. Conf. Ser. Iop Publ.* **2022**, *2258*, 012066. [\[CrossRef\]](#)
- Yang, T.C. Deconvolved Conventional Beamforming for a Horizontal Line Array. *IEEE J. Ocean. Eng.* **2018**, *43*, 160–172. [\[CrossRef\]](#)
- Yang, T.C. Deconvolution of decomposed conventional beamforming. *J. Acoust. Soc. Am.* **2020**, *148*, EL195–EL201. [\[CrossRef\]](#)
- Zhao, A.; Wang, K.; Hui, J.; Zeng, C.; Tang, K. Spatial Spectral Enhancement of Broadband Signals in a Towed Array Using Deconvolved Subband Peak Energy Detection. *Remote Sens.* **2022**, *14*, 3008. [\[CrossRef\]](#)
- Kaiyue, Z.; Wei, W.; Xiaolin, W. A Method to Improve Cross-azimuth Detection of Weak Targets under Strong Interference. In Proceedings of the 2021 OES China Ocean Acoustics (COA), Harbin, China, 14–17 July 2021; pp. 861–865.
- Wang, L.; Yang, Y.; Liu, X. A distributed subband valley fusion (DSVF) method for low frequency broadband target localization. *J. Acoust. Soc. Am.* **2018**, *143*, 2269–2278. [\[CrossRef\]](#) [\[PubMed\]](#)
- Li, Q.; Pan, X.; Li, Y. A New Background Equalization Algorithm in Digital Sonar. *J. Acoust.* **2000**, *1*, 5–9.
- Yin, F.; Li, C.; Wang, H.; Yang, F. Automatic Acoustic Target Detecting and Tracking on the Azimuth Recording Diagram with Image Processing Methods. *Sensors* **2019**, *19*, 5391. [\[CrossRef\]](#) [\[PubMed\]](#)
- Aharon, M.; Elad, M.; Bruckstein, A.M. On the uniqueness of overcomplete dictionaries, and a practical way to retrieve them. *Linear Algebra Appl.* **2006**, *416*, 48–67. [\[CrossRef\]](#)

19. Buades, A.; Coll, B.; Morel, J. A non-local algorithm for image denoising. In Proceedings of the 2005 IEEE Computer Society Conference on Computer Vision and Pattern Recognition (CVPR'05), San Diego, CA, USA, 20–26 June 2005; Volume 2, pp. 60–65. [[CrossRef](#)]
20. Dabov, K.; Foi, A.; Katkovnik, V.; Egiazarian, K. Image Denoising by Sparse 3-D Transform-Domain Collaborative Filtering. *IEEE Trans. Image Process.* **2007**, *16*, 2080–2095. [[CrossRef](#)]
21. Rank, K.; Lendl, M.; Unbehauen, R. Estimation of image noise variance. *IEEE Proc.-Vision, Image Process. Signal* **1999**, *146*, 80–84. [[CrossRef](#)]
22. Bilcu, R.; Vehvilainen, M. New method for noise estimation in images. In Proceedings of the NSIP 2005, IEEE-Eurasip Nonlinear Signal and Image Processing, Sapporo, Japan, 18–20 May 2005; p. 25.
23. Immerkaer, J. Fast Noise Variance Estimation. *Comput. Vis. Image Underst.* **1996**, *64*, 300–302. [[CrossRef](#)]
24. Amer, A.; Dubois, E. Fast and reliable structure-oriented video noise estimation. *IEEE Trans. Circuits Technol. Syst. Video* **2005**, *15*, 113–118. [[CrossRef](#)]
25. Donoho, D.L. De-noising by soft-thresholding. *IEEE Trans. Inf. Theory* **1995**, *41*, 613–627. [[CrossRef](#)]
26. De Stefano, A.; White, P.R.; Collis, W.B. Training methods for image noise level estimation on wavelet components. *EURASIP J. Adv. Signal Process.* **2004**, *2004*, 1–8. [[CrossRef](#)]
27. Chen, G.; Zhu, F.; Ann Heng, P. An efficient statistical method for image noise level estimation. In Proceedings of the IEEE International Conference on Computer Vision, Santiago, Chile, 7–13 December 2015; pp. 477–485.

Disclaimer/Publisher's Note: The statements, opinions and data contained in all publications are solely those of the individual author(s) and contributor(s) and not of MDPI and/or the editor(s). MDPI and/or the editor(s) disclaim responsibility for any injury to people or property resulting from any ideas, methods, instructions or products referred to in the content.

Reproduced with permission of copyright owner. Further reproduction prohibited without permission.